

Strain effect on power factor in monolayer MoS₂

San-Dong Guo

Department of Physics, School of Sciences, China University of Mining and Technology, Xuzhou 221116, Jiangsu, China

Biaxial strain dependence of electronic structures and thermoelectric properties of monolayer MoS₂, including compressive and tensile strain, are investigated by using local-density approximation (LDA) plus spin-orbit coupling (SOC). Both LDA and LDA+SOC results show that MoS₂ is a direct gap semiconductor with optimized lattice constants. It is found that SOC has important effect on power factor, which can enhance one in n-type doping, but has a obvious detrimental influence for p-type. Both compressive and tensile strain can induce direct-indirect gap transition, which produce remarkable influence on power factor. Calculated results show that strain can induce significantly enhanced power factor in n-type doping by compressive strain and in p-type doping by tensile strain at the critical strain of direct-indirect gap transition. These can be explained by strain-induced accidental degeneracies, which leads to improved Seebeck coefficient. Calculated results show that n-type doping can provide better power factor than p-type doping. These results make us believe that thermoelectric properties of monolayer MoS₂ can be improved in n-type doping by compressive strain.

PACS numbers: 72.15.Jf, 71.20.-b, 71.70.Ej, 79.10.-n

Keywords: Spin-orbit coupling; Strain; Power factor

I. INTRODUCTION

Thermoelectric material by using the Seebeck effect and Peltier effect can realize hot-electricity conversion to solve energy issues. As is well known, the efficiency of thermoelectric conversion can be characterized by dimensionless figure of merit^{1,2}, $ZT = S^2\sigma T/(\kappa_e + \kappa_L)$, where S , σ , T , κ_e and κ_L are the Seebeck coefficient, electrical conductivity, absolute temperature, the electronic and lattice thermal conductivities, respectively. Bismuth-tellurium systems^{3,4} and lead chalcogenides^{5,6} are excellent thermoelectric material in the application of thermoelectric devices. Searching for high ZT materials is the main objective of thermoelectric research, which requires a high electrical conductance and large Seebeck coefficient and low thermal conductance. However, they are generally coupled with each other. So, it is difficult to enhance one, but not to adversely affect else parameter. Low-dimensional materials have been proved to be advanced in designing high-performance thermoelectric devices, such as Bi₂Te₃ nanowire, monolayer phosphorene and silicene⁷⁻¹¹.

Semiconducting two-dimensional (2D) materials have potential application in nanoelectronics and nanophotonics. Due to the presence of intrinsic direct band gap of 1.9 eV, monolayer MoS₂ have been widely investigated both experimentally and theoretically¹²⁻¹⁸ in comparison with the gapless Graphene. Recently, it has been applied in field effect transistors, photovoltaics and photocatalysis¹⁹⁻²³. Band gap tuning is very important for electronic and photonics applications, which has been realized by applied strain and electric field²⁴⁻²⁹. The thermoelectric properties related with MoS₂ has been widely investigated, including bulk³⁰, few layers³¹, monolayers to nanotubes^{32,33} and armchair and zigzag mono- and fewlayer MoS₂³⁴. In these theoretical calculation, SOC is neglected, but SOC is very important for power

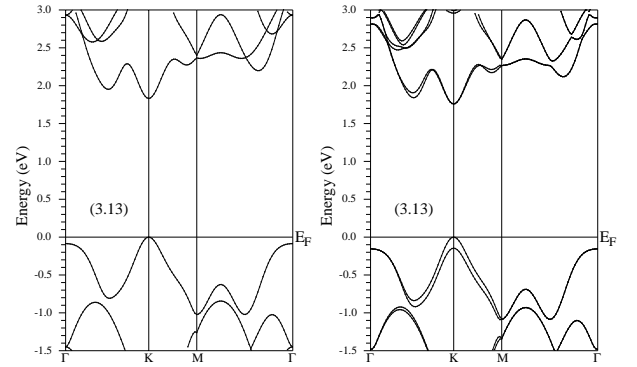


FIG. 1. The energy band structures of monolayer MoS₂ with the optimized lattice constants by using LDA (Left) and LDA+SOC (Right).

factor calculations³⁵⁻³⁷. The thermoelectric power factor can be enhanced dramatically by applied strain³⁷⁻⁴⁰ in some thermoelectric materials.

Here, the biaxial strain dependence of electronic structures and power factor of monolayer MoS₂ are calculated by first-principle calculations and Boltzmann transport theory, including the relativistic effect. Calculated results show that SOC can reduce power factor in p-type doping, and that can improve one in n-type doping, which is different from the usual detrimental effects^{35,36}. It is found that strain can induce significantly enhanced power factor in both n-type and p-type doping by tuning the electronic structures of monolayer MoS₂, which can be explained by strain-induced accidental degeneracies. Compressive strain tuning can induce better power factor in n-type doping, therefore monolayer MoS₂ can become more efficient for thermoelectric application in n-type doping.

The rest of the paper is organized as follows. In the next section, we shall give our computational details. In

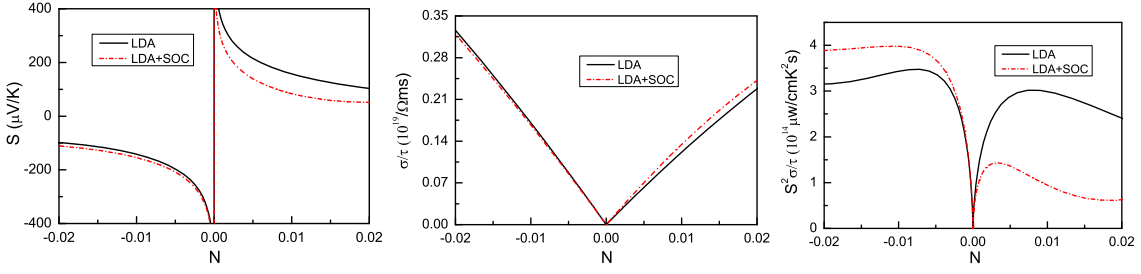


FIG. 2. (Color online) At temperature of 300 K, transport coefficients as a function of doping levels (electrons [minus value] or holes [positive value] per unit cell): Seebeck coefficient S (Left), electrical conductivity with respect to scattering time σ/τ (Middle) and power factor with respect to scattering time $S^2\sigma/\tau$ (Right) calculated with LDA (Black solid line) and LDA+SOC (Red dotted line).

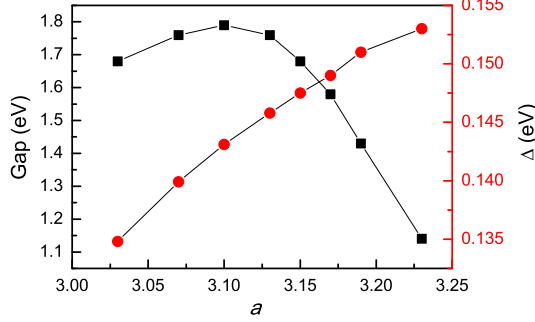


FIG. 3. (Color online) The energy band gap (Gap) and the value of spin-orbit splitting at K point (Δ) as a function of a by using LDA+SOC.

the third section, we shall present our main calculated results and analysis. Finally, we shall give our conclusion in the fourth section.

II. COMPUTATIONAL DETAIL

We use a full-potential linearized augmented-plane-waves method within the density functional theory (DFT)⁴¹, as implemented in the package WIEN2k⁴². We use LDA for the exchange-correlation potential to do our DFT calculations. The full relativistic effects are calculated with the Dirac equations for core states, and the scalar relativistic approximation is used for valence states^{43–45}. The SOC was included self-consistently by solving the radial Dirac equation for the core electrons and evaluated by the second-variation method⁴⁶. We use 6000 k-points in the first Brillouin zone for the self-consistent calculation. We make harmonic expansion up to $l_{\max} = 10$ in each of the atomic spheres, and set $R_{\text{mt}} * k_{\max} = 8$. The self-consistent calculations are considered to be converged when the integration of the absolute charge-density difference between the input and output electron density is less than $0.0001|e|$ per formula unit, where e is the electron charge. Transport calculations are performed through solving Boltzmann transport equations within the constant scattering time approxi-

mation (CSTA) as implemented in BoltzTrap⁴⁷ (Note: the parameter LPFAC can not choose the default value 5, and should choose larger value. Here, we choose LPFAC value for 20.), which has been applied successfully to several materials^{48–50}. To obtain accurate transport coefficients, we use $200 \times 200 \times 1$ k-point meshes in the first Brillouin zone for the energy band calculation.

III. MAIN CALCULATED RESULTS AND ANALYSIS

Firstly, the crystal structure of monolayer MoS_2 is constructed with the vacuum region of 20 Å to avoid spurious interaction, and the optimized lattice constant is $a=3.13$ Å by using LDA. The SOC effect on electronic structures is considered, and the energy band structures by using LDA and LDA+SOC are plotted in Figure 1. Both LDA and LDA+SOC results show MoS_2 is a direct gap semiconductor, with the band gap value being 1.87 eV and 1.76 eV, respectively. Both a and LDA gap are consistent with other theoretical values¹⁸. It is clearly seen that SOC has obvious influence on the valence bands near high symmetry K point, leading to a spin-orbital splitting value of 0.146 eV at K point, while has a negligible effect on the conduction bands near K point. However, the remarkable splitting is observed along the high symmetry Γ -K line on the conduction bands. These SOC effects produce remarkable influence on the thermoelectric properties.

The transport coefficients calculations, such as Seebeck coefficient S and electrical conductivity with respect to scattering time σ/τ , are performed within CSTA Boltzmann theory. Any assumptions on temperature and doping level dependence of the band structure are not considered. To consider SOC effects on thermoelectric properties, Figure 2 shows the Seebeck coefficient S , electrical conductivity with respect to scattering time σ/τ and power factor with respect to scattering time $S^2\sigma/\tau$ as a function of doping levels at the temperature of 300 K by using LDA and LDA+SOC. The negative doping levels imply the n-type doping, being related to conduction bands, with the negative Seebeck coefficient, and the pos-

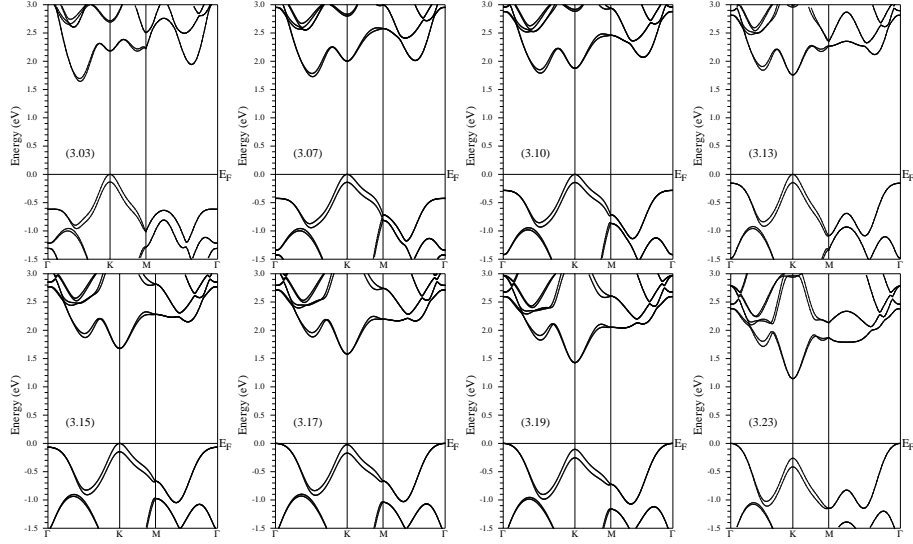


FIG. 4. The energy band structures of monolayer MoS₂ with a being from 3.03 Å to 3.23 Å calculated by using LDA+SOC.

itive doping levels mean p-type doping, being connected to the valence bands, with the positive Seebeck coefficient.

In p-type doping, SOC has a detrimental influence on the Seebeck coefficient S , while has a improved effect on S (absolute value) in n-type doping. The opposite SOC effect on the σ/τ is observed for both p-type and n-type doping. Due to the dominant role of S to power factor, the same influence of SOC on the power factor with S is found. The SOC produces larger influence on power factor in p-type than in n-type. The maximum power factors (MPF) in unit of $\tau \times 10^{14} \mu\text{W}/(\text{cmK}^2\text{s})$ are extracted in n-type and p-type doping with LDA and LDA+SOC. The MPF by using LDA+SOC in p-type doping is about 52.5% smaller than that with LDA, while the MPF with LDA+SOC is about 14.6 % bigger than that by LDA in n-type. So, the SOC has to be considered in the theoretical prediction of power factor of monolayer MoS₂.

The effects of SOC on S can be explained by analyzing SOC influence on the band structure. Upon opening of SOC, the conduction band extremum along the Γ -L line moves close to the conduction band minimum (CBM) due to the spin-orbital splitting, giving rise to more adjacent electron pockets (n-type), which induces higher S . However, SOC removes the degeneracy of valence band maximum (VBM) at the K point, reducing the slope of density of states (DOS) near the Fermi level in the valence bands (p-type), which leads to the lower S . When SOC is included, the valence bands become more dispersive, increasing the mobility of p-type charge carriers, resulting in an improved σ/τ . However, SOC has little effect on the conduction band dispersion, leading to weak dependence of SOC on σ/τ .

Strain effect on the electronic structures of monolayer MoS₂ has been widely investigated by the theoretical calculations at the absence of SOC, and semiconductor-metal phase transition has been predicted by using both

tensile and compressive strain^{25–27}. Here, we investigate the biaxial strain dependence of electronic structures and thermoelectric properties by using LDA+SOC. The energy band gap and spin-orbit splitting value at VBM as a function of a by using LDA+SOC are present in Figure 3, and the energy band structures for considered a are also displayed in Figure 4. The energy band gap firstly increases, and then decreases with increasing a . The corresponding strain changes from compressive one to tensile one. Both compressive and tensile strain can induce the direct-indirect-gap crossover, due to changing from one point of Γ -K line to K point for CBM and from K to Γ for VBM with increasing a . The spin-orbit splitting monotonically increases with the increasing a , but has little change about 0.02 eV with a varying from 3.03 Å to 3.23 Å.

The strain dependence of S , σ/τ and $S^2\sigma/\tau$ with a changing from 3.03 Å to 3.23 Å calculated by using LDA+SOC at temperature of 300 K are plotted in Figure 5. The complex dependence of strain is observed, due to the sensitive dependence of energy band structures on the applied strain. By analysing the energy band structure and the corresponding power factor, strain driven accidental degeneracies can explain strain dependence of power factor. In n-type doping, the larger S can be attained, leading to larger power factor, when the energy level of some conduction band extrema is closer. For these calculated a , the largest S and $S^2\sigma/\tau$ can be attained with $a=3.10$ Å in n-type doping due to the near degeneracy between conduction band extremum along Γ -K line and one at K point. The same mechanism can be used for p-type, and when the energy level of some valence peaks is more adjacent, the greater power factor can be gained. For p-type, S and $S^2\sigma/\tau$ reach the peak with $a=3.17$ Å, because the near degeneracy happen to be induced between Γ point and K point near the Fermi level in the valence bands. When compressive strain is applied,

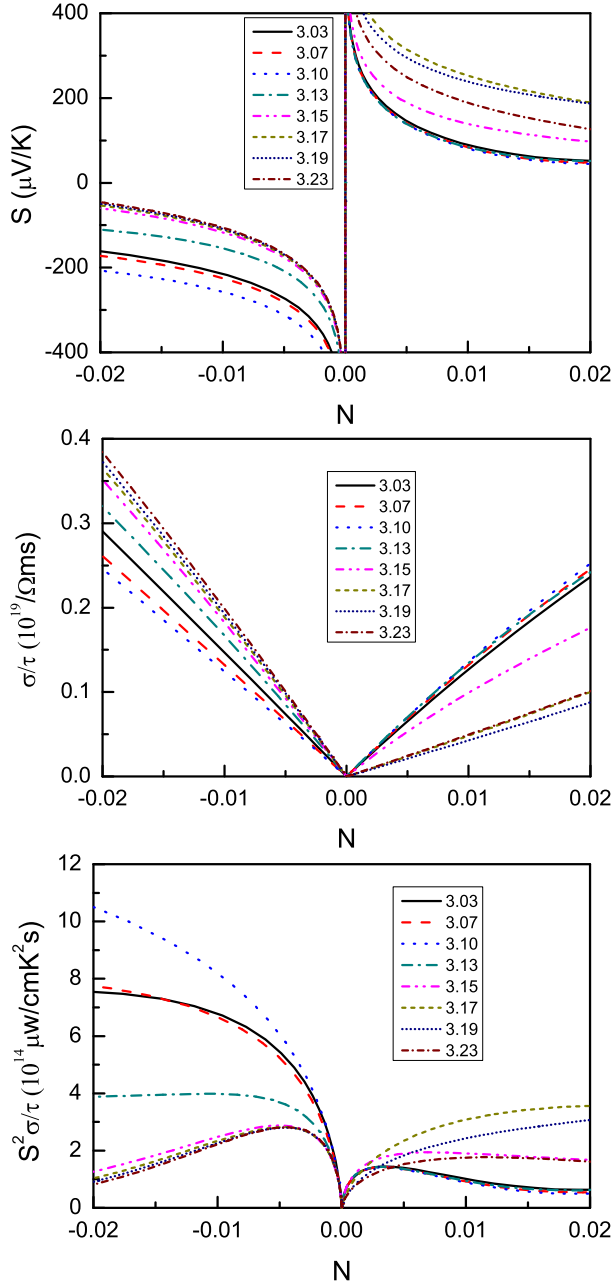


FIG. 5. (Color online) At temperature of 300 K, transport coefficients as a function of doping levels (electrons [minus value] or holes [positive value] per unit cell): Seebeck coefficient S (Top), electrical conductivity with respect to scattering time σ/τ (Middle) and power factor with respect to scattering time $S^2\sigma/\tau$ (Bottom) with a being from 3.03 Å to 3.23 Å calculated by using LDA+SOC.

the direct-indirect gap transition is induced, and the corresponding critical a can produce the largest power factor for n-type in the considered a and doping range. The tensile strain can lead to the greatest power factor for p-type at the critical a of direct-indirect gap transition. It is found that MoS₂ has larger power factor in n-type doping than in p-type doping by using compressive strain. Here,

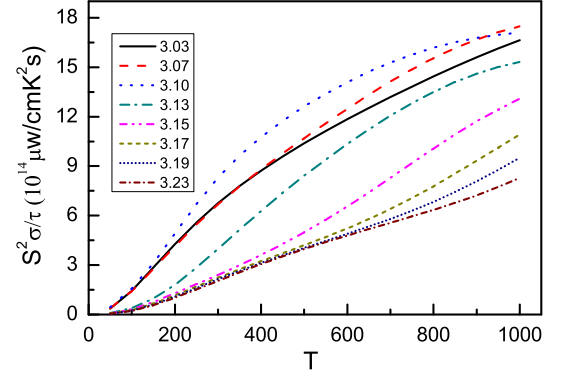


FIG. 6. (Color online) Power factor with respect to scattering time $S^2\sigma/\tau$ as a function of temperature for n-type with a being from 3.03 Å to 3.23 Å calculated by using LDA+SOC with the doping concentration of $1.23 \times 10^{13} \text{ cm}^{-2}$ (about 0.01 electrons).

the $S^2\sigma/\tau$ as a function of temperature with the doping concentration of $1.23 \times 10^{13} \text{ cm}^{-2}$ for n-type are plotted in Figure 6. In the wide temperature range, the power factor with $a=3.10$ Å is the largest among the considered a .

IV. DISCUSSIONS AND CONCLUSION

The SOC can remove the band degeneracy, which produces remarkable influence on the power factor. The SOC can lead to detrimental influence on power factor in Mg₂Sn³⁵ and half-Heusler ANiB (A=Ti, Hf, Sc, Y; B=Sn, Sb, Bi)³⁶, especially for p-type doping. For monolayer MoS₂ with optimized lattice constant, SOC not only can reduce power factor in p-type doping, but can enhance one in n-type doping. When SOC is not included, the p-type and n-type doping have the near same power factor. However, at the presence of SOC, the n-type doping shows more excellent power factor than p-type doping. So, it is very crucial for power factor calculations to consider SOC for monolayer MoS₂ in both p-type and n-type doping.

Strain or pressure is a very effective way to realize novel phenomenon by tuning the electronic structures, such as pressure-induced high-T_c superconductivity^{51,52} and strain-induced topological insulator⁵³. The sensitive strain dependence of electronic structures of monolayer MoS₂ provides a platform to tune its thermoelectric properties. The high power factor can be attained by symmetry driven degeneracy, low-dimensional electronic structures and accidental degeneracies⁵⁴. Here, the accidental degeneracies can be induced by both compressive and tensile strain at the critical strain of direct-indirect gap transition, which leads to the larger power factor in certain doping range. Similar pressure induced accidental degeneracies, leading to large power factor, can be found in Mg₂Sn at the critical pressure of energy band

gap³⁷.

As is well known, the power factor depends on the electronic energy structures. The electronic structures of monolayer MoS₂ can not only be tuned by strain, but by electric field. In Ref.²⁹, the effect of vertical electric field on the electronic structure of MoS₂ bilayer is systematically studied by the first-principle calculations, and the energy band gap monotonically decrease with the electric field increasing, leading to the semiconductor-to-metal transition. Therefore, it is possible to realize improved power factor by applied electric field.

In summary, we investigate strain dependence of thermoelectric properties of monolayer MoS₂ by using LDA+SOC, based mainly on the reliable first-principle calculations. It is found that including SOC is very important to attain reliable power factor, due to obvious

effects of SOC on the energy band structures of monolayer MoS₂. Calculated results show that strain can realize enhanced power factor at the critical strain of direct-indirect gap transition. By choosing the appropriate doping concentration, monolayer MoS₂ under compressive strain in n-type doping can provide great opportunities for efficient thermoelectricity.

ACKNOWLEDGMENTS

This work is supported by the National Natural Science Foundation of China (Grant No. 11404391). We are grateful to the Advanced Analysis and Computation Center of CUMT for the award of CPU hours to accomplish this work.

-
- ¹ Y. Pei, X. Shi, A. LaLonde, H. Wang, L. Chen and G. J. Snyder, *Nature* **473**, 66 (2011).
 - ² A. D. LaLonde, Y. Pei, H. Wang and G. J. Snyder, *Mater. Today* **14**, 526 (2011).
 - ³ W. S. Liu, Q. Y. Zhang, Y. C. Lan, S. Chen, X. Yan, Q. Zhang, H. Wang, D. Z. Wang, G. Chen and Z. F. Ren, *Adv. Energy Mater.* **1**, 577 (2011).
 - ⁴ D. K. Ko, Y. J. Kang and C. B. Murray, *Nano Lett.*, **11**, 2841 (2011).
 - ⁵ Y. Z. Pei, X. Y. Shi, A. Lalonde et al, *Nature* **473**, 66 (2011).
 - ⁶ J. Q. He, J. R. Sootsman, S. N. Girard et al, *J. Am. Chem. Soc.* **132**, 8669 (2010).
 - ⁷ J. F. Li, W. S. Liu, L. D. Zhao and M. Zhou, *NPG Asia Mater.* **2**, 152 (2010).
 - ⁸ M. G. Kanatzidis, *Chem. Mater.* **22**, 648 (2010).
 - ⁹ G. Zhang, B. Kirk, L. A. Jauregui, H. Yang, X. Xu, Y. P. Chen and Y. Wu, *Nano Lett.* **12**, 56 (2012).
 - ¹⁰ R. Fei, A. Faghaninia, R. Soklaski, J. A. Yan, C. Lo and L. Yang, *Nano Lett.* **14**, 6393 (2014).
 - ¹¹ K. Yang, S. Cahangirov, A. Cantarero, A. Rubio and R. D'Agosta, *Phys. Rev. B* **89**, 125403 (2014).
 - ¹² K. F. Mak, C. Lee, J. Hone, J. Shan, and T. F. Heinz, *Phys. Rev. Lett.* **105**, 136805 (2010).
 - ¹³ A. Splendiani, L. Sun, Y. Zhang, T. Li, J. Kim, C. Y. Chim, G. Galli and F. Wang, *Nano Lett.* **10**, 1271 (2010).
 - ¹⁴ S. W. Han, H. Kwon, et al. *Phys. Rev. B* **84**, 045409 (2011).
 - ¹⁵ S. Lebegue and O. Eriksson, *Phys. Rev. B* **79**, 115409 (2009).
 - ¹⁶ C. G. Lee, H. G. Yan, L. E. Brus, T. F. Heinz, J. Hone and S. Ryu, *ACS Nano*, **4**, 2695 (2010).
 - ¹⁷ C. Ataca, H. Sahin, E. Akturk and S. Ciraci, *J. Phys. Chem. C* **115**, 3934 (2011).
 - ¹⁸ X. D. Li, J. T. Mullen, Z. H. Jin, K. M. Borysenko, M. B. Nardelli and K. W. Kim, *Phys. Rev. B* **87**, 115418 (2013).
 - ¹⁹ S. Ghatak, A. N. Pal and A. Ghosh, *Acs Nano* **5**, 7707 (2011).
 - ²⁰ D. J. Late, B. Liu, H. R. Matte, V. P. Dravid, C. N. R. Rao, *Acs Nano* **6**, 5635 (2012).
 - ²¹ H. Qiu et al. *Appl. Phys. Lett.* **100**, 123104 (2012).
 - ²² B. Radisavljevic, A. Radenovic, J. Brivio, V. Giacometti and A. Kis, *Nature Nanotechnology* **6**, 147 (2011).
 - ²³ X. Zong et al. *J. Am. Chem. Soc.* **130**, 7176 (2008).
 - ²⁴ S. Bhattacharyya and A. K. Singh, *Phys. Rev. B* **86**, 075454 (2012).
 - ²⁵ E. Scalise, M. Houssa, G. Pourtois, V. Afanas'ev and A. Stesmans, *Nano Res.* **5**, 43 (2012).
 - ²⁶ H. Peelaers and C. G. Van de Walle, *Phys. Rev. B* **86**, 241401(R) (2012).
 - ²⁷ W. S. Yun, S. W. Han, S. C. Hong, I. G. Kim and J. D. Lee, *Phys. Rev. B* **85**, 033305 (2012).
 - ²⁸ A. Ramasubramaniam, D. Naveh and E. Towe, *Phys. Rev. B* **84**, 205325 (2011).
 - ²⁹ Q. Liu, L. Li, Y. Li, Z. Gao, Z. Chen and J. Lu, *J. Phys. Chem. C* **116**, 21556 (2012).
 - ³⁰ H. H. Guo, T. Yang, P. Tao, Y. Wang and Z. D. Zhang, *J. Appl. Phys.* **113**, 013709 (2013).
 - ³¹ S. Bhattacharyya, T. Pandey and A. K. Singh, *Nanotechnology* **25**, 465701 (2014).
 - ³² K. X. Chen, X. M. Wang, D. C. Mo and S. S. Lyu, *J. Phys. Chem. C* **2015**, **119**, 26706 (2015).
 - ³³ M. Tahir and U. Schwingenschlögl, *New Journal of Physics* **16**, 115003 (2014).
 - ³⁴ A. Arab and Q. Li, *Sci. Rep.* **5**, 13706 (2015).
 - ³⁵ K. Kutorasinski, B. Wiendlocha, J. Tobola and S. Kaprzyk, *Phys. Rev. B* **89**, 115205 (2014).
 - ³⁶ S. D. Guo, *J. Alloy. Compd.* **663**, 128 (2016).
 - ³⁷ S. D. Guo, arXiv:1601.02079.
 - ³⁸ H. Y. Lv, W. J. Lu, D. F. Shao and Y. P. Sun, *Phys. Rev. B* **90**, 085433 (2014).
 - ³⁹ S. V. Ovsyannikov and V. V. Shchennikov, *Appl. Phys. Lett.* **90**, 122103 (2007).
 - ⁴⁰ S. V. Ovsyannikov, V. V. Shchennikov, G. V. Vorontsov, A. Y. Manakov, A. Y. Likhacheva and V. A. Kulbachinskii, *J. Appl. Phys.* **104**, 053713 (2008).
 - ⁴¹ P. Hohenberg and W. Kohn, *Phys. Rev.* **136**, B864 (1964); W. Kohn and L. J. Sham, *Phys. Rev.* **140**, A1133 (1965).
 - ⁴² P. Blaha, K. Schwarz, G. K. H. Madsen, D. Kvasnicka and J. Luitz, *WIEN2k, an Augmented Plane Wave + Local Orbitals Program for Calculating Crystal Properties* (Karlheinz Schwarz Technische Universität Wien, Austria) 2001, ISBN 3-9501031-1-2
 - ⁴³ A. H. MacDonald, W. E. Pickett and D. D. Koelling, *J. Phys. C* **13**, 2675 (1980).

- ⁴⁴ D. J. Singh and L. Nordstrom, Plane Waves, Pseudopotentials and the LAPW Method, 2nd Edition (Springer, New York, 2006).
- ⁴⁵ J. Kunes, P. Novak, R. Schmid, P. Blaha and K. Schwarz, Phys. Rev. B **64**, 153102 (2001).
- ⁴⁶ D. D. Koelling, B. N. Harmon, J. Phys. C Solid State Phys. **10**, 3107 (1977).
- ⁴⁷ G. K. H. Madsen and D. J. Singh, Comput. Phys. Commun. **175**, 67 (2006).
- ⁴⁸ B. L. Huang and M. Kaviani, Phys. Rev. B **77**, 125209 (2008).
- ⁴⁹ L. Q. Xu, Y. P. Zheng and J. C. Zheng, Phys. Rev. B **82**, 195102 (2010).
- ⁵⁰ J. J. Pulikkotil, D. J. Singh, S. Auluck, M. Saravanan, D. K. Misra, A. Dhar and R. C. Budhani, Phys. Rev. B **86**, 155204 (2012).
- ⁵¹ D. F. Duan, Y. X. Liu, F. B. Tian, D. Li, X. L. Huang, Z. L. Zhao, H. Y. Yu, B. B. Liu, W. J. Tian and T. Cui, Sci. Rep. **4**, 6968 (2014).
- ⁵² A. P. Drozdov, M. I. Erements, I. A. Troyan, V. Ksenofontov and S. I. Shylin, Nature **525**, 73 (2015).
- ⁵³ W. L. Liu, X. Y. Peng, C. Tang, L. Z. Sun, K. W. Zhang, and J. X. Zhong, Phys. Rev. B **84**, 245105 (2011).
- ⁵⁴ K. F. Garrity, arXiv:1601.01622.